J|A|C|S ARTICLES

Published on Web 12/30/2009

Trends in Substrate Hydroxylation Reactions by Heme and Nonheme Iron(IV)-Oxo Oxidants Give Correlations between Intrinsic Properties of the Oxidant with Barrier Height

Sam P. de Visser*

Manchester Interdisciplinary Biocenter and School of Chemical Engineering and Analytical Science, University of Manchester, 131 Princess Street, Manchester M1 7DN, United Kingdom

Received October 1, 2009; E-mail: sam.devisser@manchester.ac.uk

Abstract: Iron(IV)-oxo species have been characterized in several nonheme enzymes and biomimetic systems and are efficient oxidants of aliphatic hydroxylation reactions. However, there appears to be a large variation in substrate hydroxylation ability by different iron(IV)-oxo oxidants due to the effect of the ligands bound to the metal. In this work, we have studied these indirect effects of ligands perpendicular (cis or equatorial) and opposite (trans or axial) to the iron(IV)-oxo group in heme and nonheme oxidants on the oxygenation capability of the oxidant. To this end, we have done a series of density functional theory calculations on the hydrogen atom abstraction of propene by a range of different iron(IV)-oxo oxidants that include heme and nonheme iron(IV)-oxo oxidants. We show that the hydrogen atom abstraction barrier of substrate hydroxylation correlates linearly with the strength of the Fe(III)O−H bond that is formed, i.e., BDE_{OH}, and that this value ranges by at least 20 kcal mol^{-1} dependent on the cis- and trans-ligands attached to the metal. Thus, our studies show that ligands bound to the metal are noninnocent and influence the catalytic properties of the metal-oxo group dramatically due to involvement into the high-lying occupied and virtual orbitals. A general valence bond curve crossing model is set up that explains how the rate constant of hydrogen atom abstraction is proportional to the difference in energy of the C−H bond of the substrate that is broken and the O−H bond of the Fe(III)O−H complex that is formed, i.e., proportional to $BDE_{CH} - BDE_{OH}$ or the reaction enthalpy. In addition, we show a correlation between the polarizability change and barrier height for the hydrogen atom abstraction reaction.

Introduction

High-valent iron(IV)-oxo species have been identified as the active oxidant of several heme and nonheme enzymes,[1] and have been shown to be able to hydroxylate C−H bonds of substrates very efficiently. The cytochromes P450, for instance, are heme-based monoxygenases involved in key biochemical reactions in the body that include detoxification processes in the liver, the biosynthesis of hormones and drug metabolism.[2] Research on P450 enzymes is hampered due to the fact that the active oxidant of these enzymes is elusive, although indirect evidence through kinetic isotope effect studies suggests that a high-valent iron(IV)-oxo heme cation radical (also known as Compound I, Cpd I) is the intermediate responsible for substrate monoxygenation.[3] These studies are supported by extensive density functional theory (DFT) and quantum mechanics/molecular mechanics (QM/MM) studies on the activity of P450 (models).[4] Reactions catalyzed by these enzymes include aliphatic and aromatic hydroxylation, *N*-dealkylation, dehydrogenation, epoxidation, and sulfoxidation.[5]

Another class of mononuclear iron containing enzymes that is involved in substrate hydroxylation are the α-ketoacid dependent dioxygenases.[6] These enzymes bind α-ketoglutarate and molecular oxygen on an iron center to generate a high-valent nonheme iron(IV)-oxo species, succinate, and carbon dioxide. Several nonheme iron(IV)-oxo complexes of enzymatic systems have been identified in recent years as well as some biomimetic iron(IV)-oxo complexes and characterized with various spectroscopic methods.[7] Despite this, the understanding of the effects of the other ligands bound to the metal on the oxygenation properties of the iron(IV)-oxo oxidant is limited. It is known that the axial ligand in heme enzymes either exerts a push-effect, e.g., in thiolate ligated systems, or a pull-effect,

(1) (a) Sono, M.; Roach, M. P.; Coulter, E. D.; Dawson, J. H. *Chem. Rev.* **1996**, *96*, 2841–2888. (b) Costas, M.; Mehn, M. P.; Jensen, M. P.; Que, L., Jr. *Chem. Rev.* **2004**, *104*, 939–986. (c) Nam, W. *Acc. Chem. Res.* **2007**, *40*, 522–531.

(2) (a) Guengerich, F. P. *Chem. Res. Toxicol.* **2001**, *14*, 611–650. (b) Groves, J. T. *Proc. Natl. Acad. Sci. U.S.A.* **2003**, *100*, 3569–3574. (c) Ortiz de Montellano, P. R., Ed. *Cytochrome P450: Structure, Mechanism and Biochemistry*, 3rd ed.; Kluwer Academic/Plenum Publishers, New York, 2005. (d) Munro, A. W.; Girvan, H. M.; McLean, K. J. *Nat. Prod. Rep.* **2007**, *24*, 585–609.

(3) (a) Egawa, T.; Shimada, H.; Ishimura, Y. *Biochem. Biophys. Res. Commun.* **1994**, *201*, 1464–1469. (b) Kellner, D. G.; Hung, S. C.; Weiss, K. E.; Sligar, S. G. *J. Biol. Chem.* **2002**, *277*, 9641–9644.

(4) (a) Loew, G. H.; Harris, D. L. *Chem. Rev.* **2000**, *100*, 407–419. (b) Shaik, S.; Kumar, D.; de Visser, S. P.; Altun, A.; Thiel, W. *Chem. Rev.* **2005**, *105*, 2279–2328.

(5) Groves, J. T. Models and mechanisms of cytochrome P450 action. In *Cytochrome P450, Structure, Mechanism and Biochemistry*; Ortiz de Montellano, P. R., Ed.; Kluwer Academic/Plenum Publishers: New York, 2005; Chapter 1, pp 1−44.

(6) (a) Solomon, E. I.; Brunold, T. C.; Davis, M. I.; Kemsley, J. N.; Lee, S.-K.; Lehnert, N.; Neese, F.; Skulan, A. J.; Yang, Y.-S.; Zhou, J. *Chem. Rev.* **2000**, *100*, 235–349. (b) Ryle, M. J.; Hausinger, R. P. *Curr. Opin. Chem. Biol.* **2002**, *6*, 193–201.

e.g., in histidine ligated complexes.[8] So far, however, a direct correlation between the ligand effect and the oxygenation properties of iron(IV)-oxo complexes has never been established. To understand the effect of metal ligand binding on the oxidative properties of high-valent iron(IV)-oxo oxidants, we have performed a series of DFT calculations on substrate hydroxylation by a range of different iron(IV)-oxo oxidants.

In principle, substrate hydroxylation proceeds in a stepwise manner with an initial hydrogen atom abstraction followed by rebound of the hydroxo group to the substrate in a consecutive step.[9] Evidence from kinetic isotope effect studies[10] shows that the rate determining step in substrate hydroxylation, however, is usually the initial hydrogen atom abstraction from a substrate (SubH) by the iron(IV)-oxo species with ligand system L, as described by eq 1, to give an iron(III)-hydroxo complex and Sub$^{\bullet}$. Thermodynamically, the reaction enthalpy (ΔH_r) of eq 1 is described by the difference in strength of the O−H bond of the iron(III)-hydroxo complex that is formed (BDE_{OH}), and the strength of the C−H bond of Sub-H, BDE_{CH}, eqs 2 and 3. Furthermore, studies of the Mayer group showed a linear correlation between BDE_{CH} and the log of the rate constant of substrate hydroxylation by several metal-oxo complexes,[11] implicating that the barrier height of the reaction follows a similar correlation to that of the overall reaction energy. Subsequently, this correlation was shown for a range of different hydrogen abstraction reactions by iron-oxo and manganese-oxo oxidants.[12] Thus, if this correlation is general than the "best" oxidant of hydrogen abstraction reactions should be the one with the largest BDE_{OH}. Borovik and co-workers have synthesized specific iron and manganese oxo complexes with the aim to create systems with large BDE_{OH} values.[13] In this work, we present a series of density functional theory (DFT) calculations on substrate hydroxylation by a range of different iron(IV)-oxo oxidants with heme as well as nonheme ligand systems and search for properties that correlate to the rate constant or the enthalpy of the barrier.

$$Fe^{IV}{=}O(L) + Sub\text{-}H \rightarrow Fe^{III}OH(L) + Sub^{\bullet} \quad (1)$$

$$\Delta H_r(\text{eq } 1) = BDE_{CH} - BDE_{OH} \quad (2)$$

$$AH \rightarrow A^{\bullet} + H^{\bullet} + BDE_{AH} \quad (3)$$

In recent studies, Shaik et al. established a valence bond (VB) curve crossing model that correlates the barrier of C−H abstraction with the strength of the C−H bond (BDE_{CH}) of the substrate and hence provided a physical explanation for the observed correlations between rate constant of hydrogen atom abstraction and BDE_{CH}.[14] These studies, however, used only one particular oxidant, namely an iron(IV)-oxo porphyrin cation radical model or Compound I (Cpd I) of P450: $Fe^{IV}{=}O(Por^{+\bullet})SH$. To establish whether a similar correlation holds for BDE_{OH} or even the difference between BDE_{CH} and BDE_{OH}, we have done a further set of calculations, where we take one particular substrate (propene) and study its aliphatic hydroxylation mechanism using a range of different iron(IV)-oxo oxidants containing heme and nonheme ligand types (L). As will be shown in this work, the factors BDE_{CH} and BDE_{OH} indeed both correlate linearly with the barrier height of hydrogen atom abstraction, which implies that the hydrogen atom abstraction barrier is also correlated with the reaction exothermicity ΔH_r.

Methods

All calculations were performed using density functional theory methods as implemented in *Jaguar 7.0* and *Gaussian-03*.[15,16] The UB3LYP hybrid density functional method[17] was used throughout and geometries were optimized (without constraints) in *Jaguar* with a double-ζ quality LACVP basis set on iron that contains a core potential and 6-31G on the rest of the atoms, basis set B1.[18] Frequency calculations use the same methods and were performed in *Gaussian−03*. Subsequent single point calculations employed a triple-ζ quality LACV3P+ basis set on iron and 6-311+G* on the rest of the atoms to improve the energetics, basis set B2. Energies reported in this work were obtained with basis set B2 and contain zero-point corrections with basis set B1.

Values for BDE_{CH} and BDE_{OH} were calculated with the same methods for consistency and are based on the energy difference as displayed in eq 3. The reorganization energy of the substrate (RE_{Sub}) was taken as the difference in energy of the geometry of the radical (Sub$^{\bullet}$) in the transition state with respect to its fully optimized structure.[19] In a similar way, the reorganization energy of the iron-hydroxo complex (RE_{FeOH}) was calculated between the difference in energy of this moiety in the transition state with respect to the fully optimized geometry.

Our work uses a selection of different iron(IV)-oxo complexes containing nonheme and heme ligand types, see Figure 1. Models

(7) (a) See, for example: Proshlyakov, D. A.; Henshaw, T. F.; Monterosso, G. R.; Ryle, M. J.; Hausinger, R. P. *J. Am. Chem. Soc.* **2004**, *126*, 1022–1023. (b) Riggs-Gelasco, P. J.; Price, J. C.; Guyer, R. B.; Brehm, J. H.; Barr, E. W.; Bollinger, J. M., Jr.; Krebs, C. *J. Am. Chem. Soc.* **2004**, *126*, 8108–8109. (c) Bukowski, M. R.; Koehntop, K. D.; Stubna, A.; Bominaar, E. L.; Halfen, J. A.; Münck, E.; Nam, W.; Que Jr., L. *Science* **2005**, *310*, 1000–1002.

(8) (a) Dawson, J. H.; Holm, R. H.; Trudell, J. R.; Barth, G.; Linder, R. E.; Bunnenberg, E.; Djerassi, C.; Tang, S. C. *J. Am. Chem. Soc.* **1976**, *98*, 3707–3709. (b) Poulos, T. L. *J. Biol. Inorg. Chem.* **1996**, *1*, 356–359.

(9) (a) Groves, J. T.; McClusky, G. A. *J. Am. Chem. Soc.* **1976**, *98*, 859–861. (b) Ortiz de Montellano, P. R.; Stearns, R. A. *J. Am. Chem. Soc.* **1987**, *109*, 3415–3420.

(10) (a) Gelb, M. H.; Heimbrook, D. C.; Malkonen, P.; Sligar, S. G. *Biochemistry* **1982**, *21*, 370–377. (b) Ortiz de Montellano, P. R.; Stearns, R. A. *J. Am. Chem. Soc.* **1987**, *109*, 3415–3420. (c) Dolphin, D.; Traylor, T. G.; Xie, L. Y. *Acc. Chem. Res.* **1997**, *30*, 251–259. (d) Goh, Y. M.; Nam, W. *Inorg. Chem.* **1999**, *38*, 914–920.

(11) (a) Mayer, J. M. *Acc. Chem. Res.* **1998**, *31*, 441–450. (b) Mayer, J. M. *Annu. Rev. Phys. Chem.* **2004**, *55*, 363–390. (c) Mader, E. A.; Manner, V. W.; Markle, T. F.; Wu, A.; Franz, J. A.; Mayer, J. M. *J. Am. Chem. Soc.* **2009**, *131*, 4335–4345.

(12) (a) Kaizer, J.; Klinker, E. J.; Oh, N. Y.; Rohde, J.-U.; Song, W. J.; Stubna, A.; Kim, J.; Münck, E.; Nam, W.; Que, L., Jr. *J. Am. Chem. Soc.* **2004**, *126*, 472–473. (b) Yoon, J.; Wilson, S. A.; Jang, Y. K.; Seo, M. S.; Nehru, K.; Hedman, B.; Hodgson, K. O.; Bill, E.; Solomon, E. I.; Nam, W. *Angew. Chem., Int. Ed.* **2009**, *48*, 1257–1260. (c) Lansky, D. E.; Goldberg, D. P. *Inorg. Chem.* **2006**, *45*, 5119–5125. (d) Goldberg, D. P. *Acc. Chem. Res.* **2007**, *40*, 626–634. (e) McGown, A. J.; Kerber, W. D.; Fujii, H.; Goldberg, D. P. *J. Am. Chem. Soc.* **2009**, *131*, 8040–8048. (f) Bell, S. R.; Groves, J. T. *J. Am. Chem. Soc.* **2009**, *131*, 9640–9641. (g) Kang, Y.; Chen, H.; Jeong, Y. J.; Lai, W.; Bae, E. H.; Shaik, S.; Nam, W. *Chem.−Eur. J.* **2009**, *15*, 10039–10046.

(13) (a) Gupta, R.; MacBeth, C. E.; Young, V. G.; Borovik, A. S. *J. Am. Chem. Soc.* **2002**, *124*, 1136–1137. (b) Gupta, R.; Borovik, A. S. *J. Am. Chem. Soc.* **2003**, *125*, 13234–13242. (c) Borovik, A. S. *Acc. Chem. Res.* **2005**, *38*, 54–61. (d) Parsell, T. H.; Yang, M.-Y.; Borovik, A. S. *J. Am. Chem. Soc.* **2009**, *131*, 2762–2763.

(14) Shaik, S.; Kumar, D.; de Visser, S. P. *J. Am. Chem. Soc.* **2008**, *130*, 10128–10140.

(15) *Jaguar 7.0*, Schrödinger, LLC.: New York, NY, 2007.

(16) Frisch, M. J. et al. *Gaussian-03*, Wallingford PA, 2003. Full reference, see Supporting Information.

(17) (a) Becke, A. D. *J. Chem. Phys.* **1993**, *98*, 5648–5652. (b) Lee, C.; Yang, W.; Parr, R. G. *Phys. Rev. B* **1988**, *37*, 785–789.

(18) Hay, P. J.; Wadt, W. R. *J. Chem. Phys.* **1985**, *82*, 270–283.

(19) Latifi, R.; Bagherzadeh, M.; de Visser, S. P. *Chem.−Eur. J.* **2009**, *15*, 6651–6662.

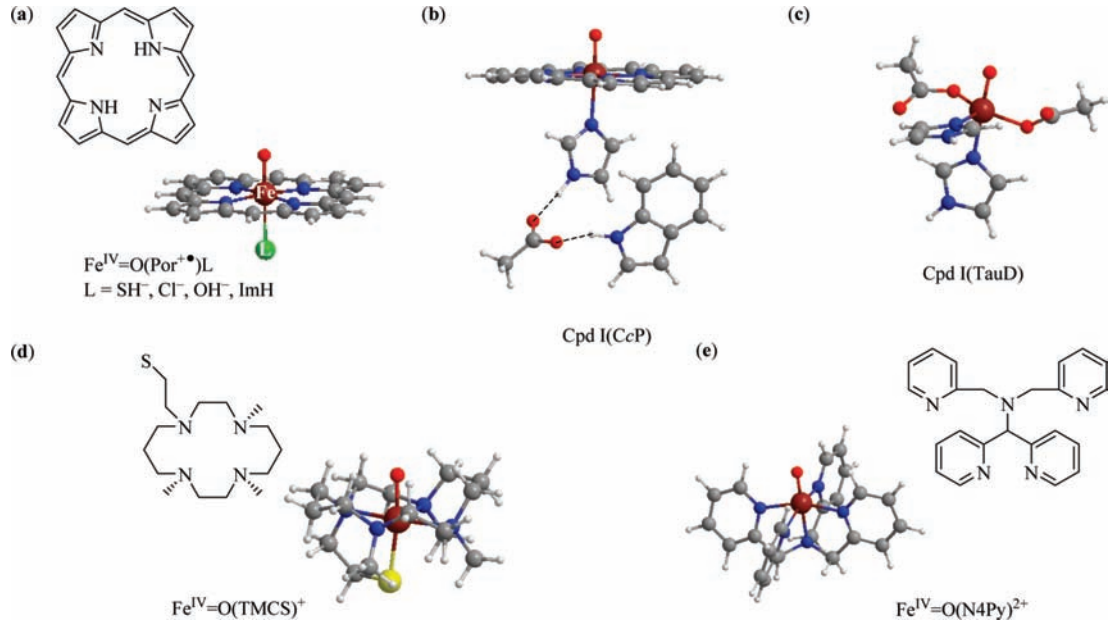

Figure 1. Iron(IV)-oxo oxidants studied in this work: (a) porphyrin based oxidants Fe^{IV}=O(Por$^{+\bullet}$)L with L = SH$^-$, Cl$^-$, OH$^-$, or ImH. (b) Cpd I model of C*c*P. (c) Cpd I model of TauD. (d) Fe^{IV}=O(TMCS)$^+$ and (e) Fe^{IV}=O(N4Py)$^{2+}$.

of P450 and horseradish peroxidase (HRP) follow previously described structures from the literature and contain protoporphyrin IX without side chains (Por) and either thiolate (SH$^-$) or imidazole (ImH) as axial ligands.[20] In addition, a biomimetic porphyrin model with chloride axial ligand was used.[21] Data for propene hydroxylation by porphyrin (Por) containing iron(IV)-oxo complexes, Fe^{IV}=O(Por$^{+\bullet}$)L with L = SH$^-$, Cl$^-$ or imidazole (ImH), were taken from the literature.[21,22] To test whether hydrogen bonding interactions toward the thiolate influence BDE_{OH}, we ran a subsequent set of calculations on a large iron(IV)-oxo model of P450 with an extensive axial ligand group including cysteinate and the subsequent three amino acids mimicked by Gly residues attached. These studies showed that BDE_{OH} of the large axial ligand model is within 1 kcal mol^{-1} of that obtained for Fe^{IV}=O(Por$^{+\bullet}$)SH. Therefore, the small P450 model with thiolate axial ligand is a good representation of the enzyme. Nonheme iron(IV)-oxo complexes include a taurine/α-ketoglutarate dioxygenase (TauD) model [Cpd I(TauD)], and a biomimetic system with 1-mercaptoethyl-4,8,11-trimethyl-1,4,8,11-tetraazacyclotetradecane (TMCS) ligand system [Fe^{IV}=O(TMCS)$^+$].[23] In addition, we ran a new set of calculations on propene hydroxylation with several iron(IV)-oxo complexes in order to enlarge the data set and the range of BDE_{OH} values. These calculations used the following Cpd I models: (i) a cytochrome *c* peroxidase (C*c*P) mimic [Cpd I(C*c*P)], (ii) Fe^{IV}=O(Por$^{+\bullet}$)OH and (iii) Fe^{IV}=O(N4Py)$^{2+}$, whereby N4Py = *N*,*N*-bis(2-pyridylmethyl)-bis(2-pyridyl)methylamine). This gives a total of eight iron(IV)-oxo oxidants for which the hydroxylation reaction of the aliphatic group of propene was investigated. The C*c*P Cpd I model is an iron(IV)-oxo species embedded in a porphyrin group and with an axial imidazole ligand replacing a histidine residue, but in addition the model also contains the hydrogen bonded axial triad of a carboxylic acid group (replaced by acetate) for Asp_{235} and an indole group for Trp_{191} (Figure 1).

Results

Substrate Hydroxylation by Iron(IV)-Oxo Oxidants. Aliphatic hydroxylation of propene by the eight different iron(IV)-oxo oxidants shown in Figure 1 is investigated. Electronically, these eight oxidants show many similarities; in particular, all oxidants have the same set of valence orbitals that determine their reactivity patterns. Let us first summarize the relevant molecular orbitals in the reaction mechanism. Figure 2 depicts the high-lying occupied and low-lying virtual orbitals of Fe^{IV}=O(Por$^{+\bullet}$)(SH) as an example. All heme oxidants studied in this work have similar molecular orbitals and occupation except Cpd I(C*c*P) which has a tryptophan radical rather than a singly occupied a_{2u} orbital. Nonheme oxidants have metal-type orbitals that resemble the metal-based 3*d* orbitals in Figure 2 closely, therefore, we will use the same orbital labeling for heme and nonheme iron(IV)-oxo oxidants. The orbitals on the left-hand-side of Figure 2 represent the metal-based orbitals of which the $\delta_{x2\text{-}y2}$ is a nonbonding orbital in the plane of the porphyrin, whereas the pair of π^*_{FeO} (π^*_{xz} and π^*_{yz}) orbitals are built up from the antibonding combination of the metal $3d_{xz}$/$3d_{yz}$ orbitals with the $2p_x$/$2p_y$ atomic orbitals on oxygen. Two virtual σ^* orbitals reflect the antibonding combinations of the metal $3d_{xy}$ with the pyrrole nitrogen atoms of the porphyrin ring (in σ^*_{xy}) and the metal $3d_{z2}$ orbital with σ-orbitals on the oxo and axial ligand groups (in σ^*_{z2}). Iron(IV)-oxo porphyrin cation radical oxidants, in addition, have two high-lying porphyrin orbitals that in D_{4h} symmetry have the labels a_{1u} and a_{2u},[24] of which the former is doubly occupied. The a_{2u} orbital, however, is singly occupied and coupled to unpaired electrons in the π^*_{xz} and π^*_{yz} orbitals in a ferromagnetic fashion to give an overall quartet spin state or antiferromagnetically coupled into a doublet spin state. These two spin states are close in energy and their

(20) de Visser, S. P.; Shaik, S.; Sharma, P. K.; Kumar, D.; Thiel, W. *J. Am. Chem. Soc.* **2003**, *125*, 15779–15788.
(21) de Visser, S. P. *J. Biol. Inorg. Chem.* **2006**, *11*, 168–178.
(22) (a) de Visser, S. P.; Ogliaro, F.; Sharma, P. K.; Shaik, S. *Angew. Chem., Int. Ed.* **2002**, *41*, 1947–1951. (b) de Visser, S. P.; Ogliaro, F.; Sharma, P. K.; Shaik, S. *J. Am. Chem. Soc.* **2002**, *124*, 11809–11826. (c) Kumar, D.; de Visser, S. P.; Sharma, P. K.; Derat, E.; Shaik, S. *J. Biol. Inorg. Chem.* **2005**, *10*, 181–189.
(23) (a) de Visser, S. P. *Angew. Chem., Int. Ed.* **2006**, *45*, 1790–1793. (b) de Visser, S. P. *J. Am. Chem. Soc.* **2006**, *128*, 9813–9824. (c) de Visser, S. P. *J. Am. Chem. Soc.* **2006**, *128*, 15809–15818.
(24) (a) Ghosh, A. *Acc. Chem. Res.* **1998**, *31*, 189–191. (b) Ogliaro, F.; de Visser, S. P.; Cohen, S.; Kaneti, J.; Shaik, S. *ChemBioChem* **2001**, *11*, 848–851.

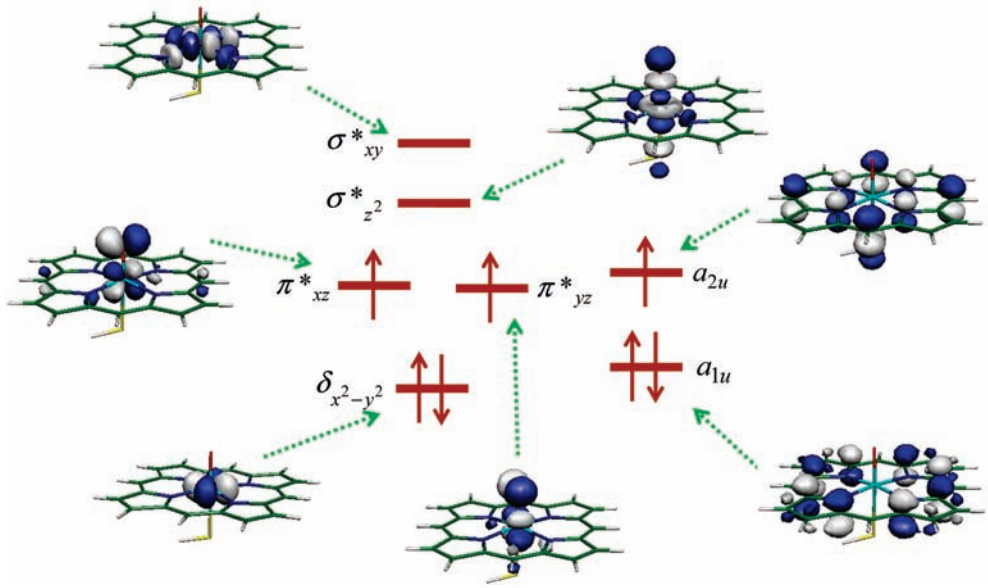

Figure 2. High-lying occupied and low-lying virtual orbitals of Cpd I(SH).

degeneracy gives rise to two-state-reactivity patterns with reaction mechanisms and barriers on both spin state surfaces.[25] In nonheme iron(IV)-oxo oxidants, the five orbitals on the left-hand-side of Figure 2 are still occupied by four electrons leading to either a triplet spin ground state with $\delta_{x2\text{-}y2}^2\ \pi^*_{xz}{}^1\ \pi^*_{yz}{}^1$ occupation or a quintet spin ground state with $\delta_{x2\text{-}y2}^1\ \pi^*_{xz}{}^1\ \pi^*_{yz}{}^1\ \sigma^*_{xy}{}^1$ occupation. Also reaction mechanisms by nonheme iron(IV)-oxo oxidants give two-state-reactivity patterns although the competing triplet and quintet spin state surfaces often give significant differences in barrier heights.[26]

Let us start with a brief summary of the observed reaction mechanisms of propene hydroxylation by the eight iron(IV)-oxo oxidants, which resemble previous studies of hydrogen atom abstraction reactions of these and similar oxidants.[27] In all cases, the iron(IV)-oxo oxidant reacts with propene to form propenol products via a stepwise mechanism that passes a radical intermediate (Figure 3). The reaction starts with an initial hydrogen atom abstraction via a hydrogen atom abstraction transition state ($\mathbf{TS}_{\mathrm{H}}$) to form a radical intermediate comprised of an iron(IV)-hydroxo-porphyrin complexed to a nearby allyl radical (RadInt). A radical rebound barrier ($\mathbf{TS}_{\mathrm{reb}}$) separates this intermediate from the alcohol product complex (Prod). Figure 3 gives a typical example of a propene hydroxylation reaction mechanism in this case using $^{4,2}\mathrm{Fe^{IV}}$═O($\mathrm{Por^{+\bullet}}$)OH as an oxidant.

Thus, iron(IV)-oxo porphyrin cation radical complexes similar to Cpd I of P450 appear in close lying doublet and quartet spin states both with the same orbital occupation $^{4,2}\mathrm{A}_{2u} = \delta_{x2\text{-}y2}^2\ \pi^*_{xz}{}^1\ \pi^*_{yz}{}^1\ a_{2u}{}^1$.[24] A subsequent hydrogen atom abstraction by this oxidant leads to formation of a radical intermediate with electronic configuration $\mathrm{Fe^{IV}}$(OH)(Por)(OH)−Sub$^\bullet$ and orbital occupation $\delta_{x2\text{-}y2}^2\ \pi^*_{xz}{}^1\ \pi^*_{yz}{}^1\ a_{2u}{}^2\ \phi_{\mathrm{Sub}}{}^1$, whereby the latter orbital represents the radical on the substrate. Subsequent radical rebound to form propenol products leads to a second electron transfer from substrate to oxidant, whereby in the low-spin an electron is moved into the π^*_{xz} orbital, while in the high-spin the σ^*_{z2} is filled with one electron.

The results shown in Figure 3 are in line with previously published studies on substrate hydroxylation reactions by iron(IV)-oxo porphyrin cation radical oxidants.[27] The doublet and quartet spin reactants are within 1 kcal mol^{-1} and the potential energy surfaces of these two spin states stay close in energy toward the intermediate complexes. Note that the hydrogen abstraction barrier of propene by $\mathrm{Fe^{IV}}$═O($\mathrm{Por^{+\bullet}}$)OH is one of the lowest hydrogen abstraction barriers observed so far as also found by recent studies of Nam et al.[12g] Also shown in Figure 3 are optimized geometries of the critical points along the reaction mechanism, which resemble those obtained from previous studies of aliphatic hydroxylation reactions.[27] The hydrogen atom abstraction transition states ($^{4,2}\mathbf{TS}_{\mathrm{H}}$) give an almost linear O−H−C angle on both spin state surfaces with the hydrogen atom almost midway in between these heavy atoms. Generally, the differences in geometry between the doublet and quartet spin state structures are small especially in the first step of the reaction mechanism. The only significant differences are found for the rebound process, which encounters a higher barrier on the high-spin surface as compared to the low-spin surface,[28] and in the two Fe−O distances for the product complexes due to differences in orbital occupation.[29]

Nonheme iron(IV)-oxo oxidants follow an analogous reaction mechanism to the heme based oxidants shown in Figure 3,

(25) Shaik, S.; de Visser, S. P.; Ogliaro, F.; Schwarz, H.; Schröder, D. *Curr. Opin. Chem. Biol.* **2002**, *6*, 556–567.
(26) Kumar, D.; Hirao, H.; Que Jr, L.; Shaik, S. *J. Am. Chem. Soc.* **2005**, *127*, 8026–8027.
(27) (a) Ogliaro, F.; Harris, N.; Cohen, S.; Filatov, M.; de Visser, S. P.; Shaik, S. *J. Am. Chem. Soc.* **2000**, *122*, 8977–8989. (b) Kamachi, T.; Yoshizawa, K. *J. Am. Chem. Soc.* **2003**, *125*, 4652–4661. (c) Kumar, D.; de Visser, S. P.; Shaik, S. *J. Am. Chem. Soc.* **2003**, *125*, 13024–13025. (d) Kumar, D.; de Visser, S. P.; Sharma, P. K.; Cohen, S.; Shaik, S. *J. Am. Chem. Soc.* **2004**, *126*, 1907–1920. (e) de Visser, S. P.; Kumar, D.; Cohen, S.; Shacham, R.; Shaik, S. *J. Am. Chem. Soc.* **2004**, *126*, 8362–8363. (f) Siegbahn, P. E. M.; Borowski, T. *Acc. Chem. Res.* **2006**, *39*, 729–738. (g) Olsen, L.; Rydberg, P.; Rod, T. H.; Ryde, U. *J. Med. Chem.* **2006**, *49*, 6489–6499. (h) Schöneboom, J. C.; Cohen, S.; Lin, H.; Shaik, S.; Thiel, W. *J. Am. Chem. Soc.* **2004**, *126*, 4017–4034. (i) de Visser, S. P. *Chem.—Eur. J.* **2006**, *12*, 8168–8177. (j) Zhang, Y.; Morisetti, P.; Kim, J.; Smith, L.; Lin, H. *Theor. Chem. Acc.* **2008**, *121*, 313–319. (k) Kumar, D.; Tahsini, L.; de Visser, S. P.; Kang, H. Y.; Kim, S. J.; Nam, W. *J. Phys. Chem. A* **2009**, *113*, 11713–11722.
(28) Shaik, S.; Cohen, S.; de Visser, S. P.; Sharma, P. K.; Kumar, D.; Kozuch, S.; Ogliaro, F.; Danovich, D. *Eur. J. Inorg. Chem.* **2004**, 207–226.
(29) de Visser, S. P.; Ogliaro, F.; Harris, N.; Shaik, S. *J. Am. Chem. Soc.* **2001**, *123*, 3037–3047.

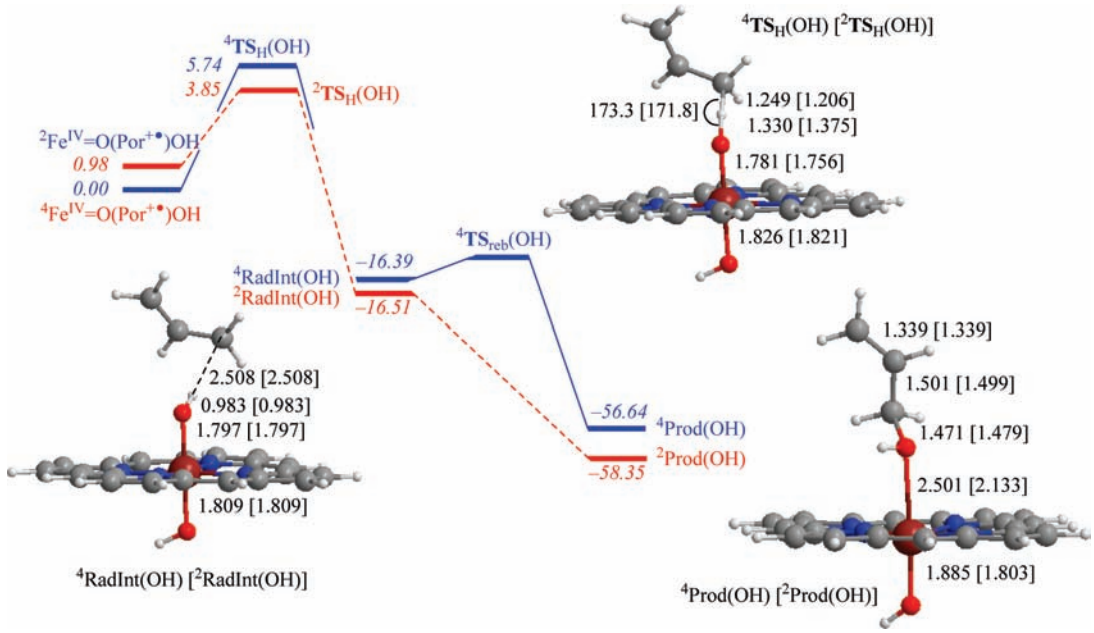

Figure 3. Potential energy profile of aliphatic hydroxylation of propene by ^{4,2}Fe^{IV}=O(Por$^{+\bullet}$)OH with energies (ΔE + ZPE) in kcal mol^{-1}. Also shown are optimized geometries of radical intermediates, alcohol product complexes and hydrogen atom abstraction transition states (**TS**$_H$) with bond lengths in angstroms and angles in degrees.

whereby an initial hydrogen atom abstraction leads to an Fe(III)-hydroxo complexed to a radical group that rebounds to form the Fe(II) product complex. The nonheme iron(IV)-oxo oxidants, however, have either a triplet spin ground state with orbital occupation $\delta_{x2\text{-}y2}^2\ \pi^*_{xz}{}^1\ \pi^*_{yz}{}^1$ or a quintet spin ground state with $\delta_{x2\text{-}y2}^1\ \pi^*_{xz}{}^1\ \pi^*_{yz}{}^1\ \sigma^*_{xy}{}^1$ occupation. All enzymatic nonheme iron(IV)-oxo complexes characterized so far have a quintet spin ground state, while synthetic biomimetic complexes usually have a triplet spin ground state, although the Fe^{IV}=O(TMCS)$^+$ system is an exception to this rule with a quintet spin ground state.[30] Nonetheless, also nonheme iron(IV)-oxo oxidants react via TSR patterns but on competing triplet and quintet spin state surfaces.[26] The doublet and quartet spin hydrogen abstraction barriers in the porphyrin ligated iron(IV)-oxo complexes are close in energy, typically within 2 kcal mol^{-1}, whereas the energy separation between the triplet and quintet spin hydrogen abstraction barriers of the nonheme iron(IV)-oxo oxidants is sometimes considerable. This is because the triplet and quintet spin states in nonheme iron(IV)-oxo complexes encounter different electron transfer processes, while the doublet and quartet spin states of porphyrin based iron(IV)-oxo complexes follow the same electron transfer mechanisms for aliphatic hydrogen atom abstraction.

Figure 4 depicts optimized geometries of ^{3,5}**TS**$_H$ of the reaction of Fe^{IV}=O(TMCS)$^+$ with propene, i.e., ^{3,5}**TS**$_H$(TMCS). Thus, in the quintet spin state the substrate approaches the oxidant from the top due to electron transfer from the substrate into the σ^*_{z2} orbital that is located along the Fe−O axis.[23b,31] In the triplet spin state, by contrast, the electron transfer is into the π^*_{xz} orbital and hence the substrate approaches the oxidant sideways. Indeed an Fe−O−H angle of 176.6° is found in ^{5}**TS**$_H$ while a value of 143.1° in ^{3}**TS**$_H$ was calculated in support with

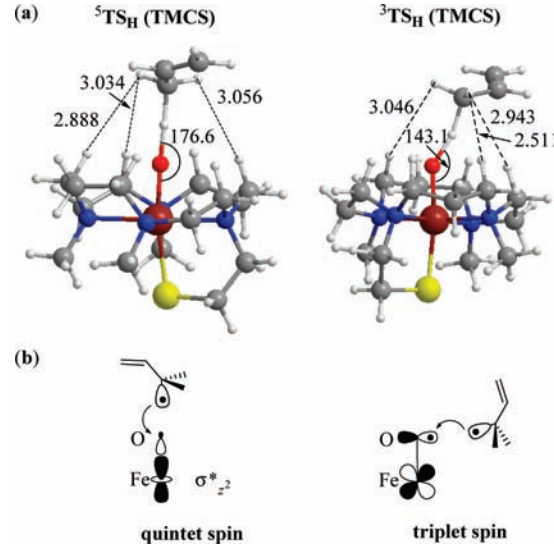

Figure 4. (a) Optimized geometries of ^{3,5}**TS**$_H$(TMCS) as taken from ref 23b. (b) Electron transfer processes in the quintet and triplet spin states.

these electron transfer mechanisms. The lowest hydrogen abstraction barrier by nonheme iron(IV)-oxo oxidants is usually on the quintet spin state surface with the triplet spin state well higher in energy, therefore we will focus our studies here on the quintet spin mechanism for the nonheme oxidants only. In the case of Fe^{IV}=O(TMCS)$^+$ the energy difference between ^{5}**TS**$_H$ and ^{3}**TS**$_H$ is larger than 10 kcal mol^{-1}, due to interactions of the protons of the TMCS ligand with protons of the substrate.[23b] Since the substrate approaches sideways in ^{3}**TS**$_H$ the repulsive interactions are larger than those for ^{5}**TS**$_H$ where the substrate approaches from the top.

For all oxidants shown in Figure 1 we calculated the hydrogen atom abstraction reaction of propene. In principle, a hydrogen atom abstraction from a substrate by an iron(IV)-oxo species leads to radical intermediates as described by eq 1 above and should have a reaction enthalpy for reactants to radical

(30) Bukowski, M. R.; Koehntop, K. D.; Stubna, A.; Bominaar, E. L.; Halfen, J. A.; Münck, E.; Nam, W.; Que, L., Jr. *Science* **2005**, *310*, 1000–1002.
(31) Decker, A.; Rohde, J.-U.; Klinker, E. J.; Wong, S. D.; Que Jr, L.; Solomon, E. I. *J. Am. Chem. Soc.* **2007**, *129*, 15983–15996.

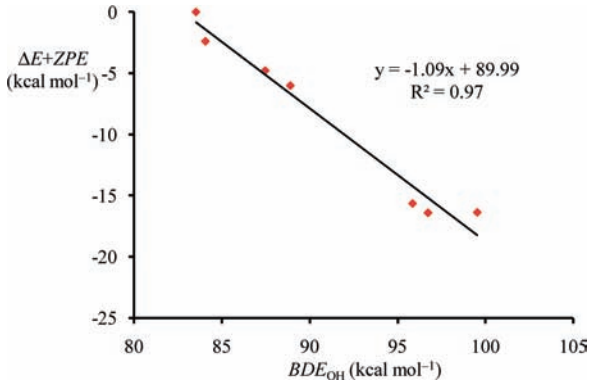

Figure 5. Correlation between reaction exothermicity for the formation of radical intermediate complex from isolated reactants with BDE_{OH}. All energetics obtained with UB3LYP/B2//UB3LYP/B1 with zero-point energies included at UB3LYP/B1.

Table 1. DFT Calculated Hydrogen Abstraction Barriers for Propene Hydroxylation by Selected Iron(IV)-Oxo Oxidants and the Calculated Values of BDE_{OH}, RE_{Sub}, RE_{FeOH}, and $EA_{Cpd\ I}$[a]

oxidant	$^{HS}TS_H$[b]	BDE_{OH}	RE_{Sub}	RE_{FeOH}	$EA_{Cpd\ I}$[c]
Fe^{IV}=O($Por^{+\bullet}$)ImH^+	15.6	80.8	−6.6	−26.2	148
Cpd I(*Cc*P)	18.4	83.5	−3.1	−22.6	148
Fe^{IV}=O(TMCS)$^+$	15.0	84.1	−7.9	−22.5	125
Fe^{IV}=O($Por^{+\bullet}$)Cl	12.9	87.5	−6.6	−23.0	79
Fe^{IV}=O($Por^{+\bullet}$)SH	13.0	88.9	−6.6	−20.7	71
Cpd I(TauD)	5.4	95.9	−9.9	−28.4	53
Fe^{IV}=O(N4Py)$^{2+}$	7.2	96.7	−5.4	−24.2	205
Fe^{IV}=O($Por^{+\bullet}$)OH	3.9	99.5	−8.1	−30.0	76
BDE_{CH} (propene)		82.6			

[a] All values are in kcal mol^{-1} and calculated at UB3LYP/B2//UB3LYP/B1 with ZPE corrections included at UB3LYP/B1. [b] High-spin (HS) barrier, i.e. quartet spin for heme systems and quintet spin for nonheme systems. [c] Electron affinity of the iron(IV)-oxo species.

intermediates that correlates with the difference between BDE_{CH} and BDE_{OH}, eq 2. Indeed a plot of the reaction energy (ΔH_r) for formation of the radical intermediates from reactants gives a linear correlation with BDE_{OH} (Figure 5) with a slope close to unity and a correlation of $R^2 = 0.97$. The intercept deviates from the calculated value of BDE_{CH} for propene of 82.6 kcal mol^{-1} due to the fact that the radical intermediates were calculated as a complex of the radical with an iron-hydroxo moiety rather than as isolated entities. Nevertheless, the correlation coefficient is excellent and shows that the calculations are reliable and that the reaction exothermicity follows thermodynamic rules.

Correlations of Barrier Height with BDE_{OH}. Table 1 summarizes the hydrogen abstraction barriers of propene hydroxylation by the eight oxidants shown in Figure 1 as well as the BDE_{OH} value of each oxidant and the calculated values of RE_{Sub} and RE_{FeOH} for the transition states structures. Figure 6 displays the calculated hydrogen abstraction barriers of propene as a function of BDE_{OH} (panel (a)) as well as BDE_{OH} corrected with the reorganization energy (RE_{Sub}) of the substrate (panel (b)) and for BDE_{OH} corrected with RE_{Sub} and RE_{FeOH} (panel (c)) for the eight iron(IV)-oxo oxidants. The correlation is fair for BDE_{OH} and improves considerably with RE_{Sub} included, similarly to what was found before for BDE_{CH}.[14] Inclusion of contribution for RE_{FeOH} gives little improvement of the correlation but is an improvement with respect to BDE_{OH} only. Therefore, the correlations shown in Figure 6 implicate a linear correlation between the hydrogen abstraction barrier and BDE_{OH}.

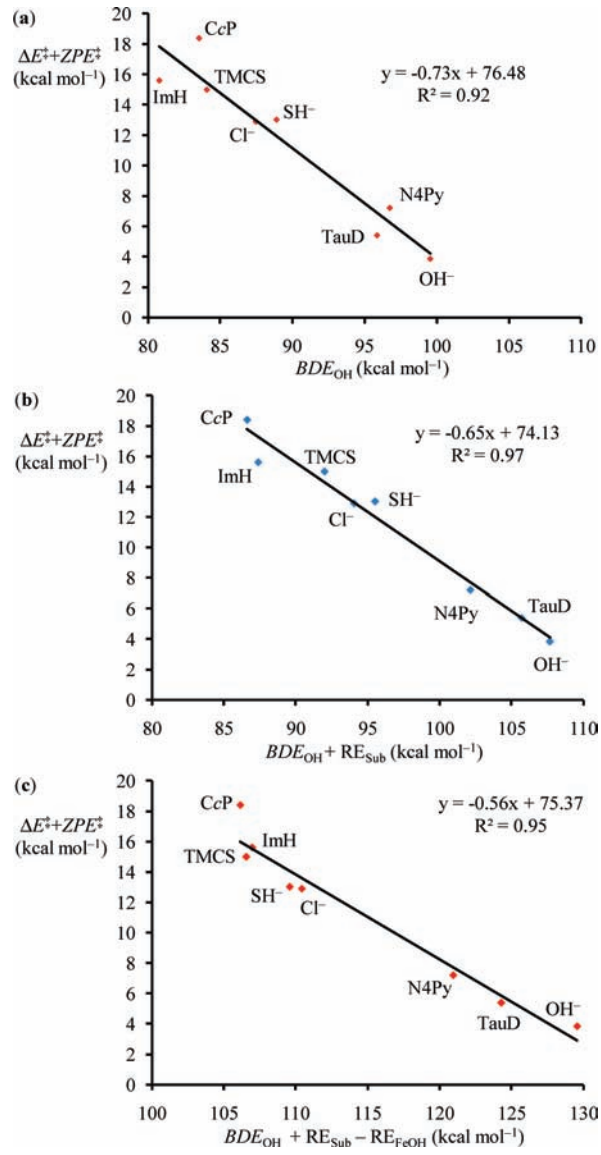

Figure 6. Barrier height of hydrogen abstraction of propene by iron(IV)-oxo complexes ($\Delta E^{\ddagger} + ZPE^{\ddagger}$) as a function of (a) BDE_{OH}, (b) $BDE_{OH} + RE_{Sub}$, and (c) $BDE_{OH} + RE_{Sub} - RE_{FeOH}$. The oxidants tested were Fe^{IV}=O($Por^{+\bullet}$)L with L = SH^-, Cl^-, OH^-, and ImH, Cpd I(*Cc*P), Cpd I(TauD), Fe^{IV}=O(TMCS)$^+$, and Fe^{IV}=O(N4Py)$^{2+}$.

Note that the oxidants tested in this work span a range of almost 20 kcal mol^{-1} in BDE_{OH}, which means that *the strength of the O−H bond in Fe(III)O−H is dramatically affected by the nature of the other bonds to the metal*, i.e., the cis and trans ligands to the oxo group. The heme models with the weakest BDE_{OH} values and consequently highest reaction barriers contain an imidazole axial ligand of a histidine residue. However, an iron(IV)-oxo porphyrin cation radical oxidant with an axial thiolate ligand (as appears in the cytochromes P450 as a cysteinate ligand) increases the BDE_{OH} by at least 8 kcal mol^{-1} with respect to Fe^{IV}=O($Por^{+\bullet}$)ImH to 88.9 kcal mol^{-1}. Test calculations with an enhanced axial ligand description with cysteinate covalently linked to two subsequent amino acids in the peptide (mimicked by Gly residues) gave a BDE_{OH} = 88.95 kcal mol^{-1}, which implies that hydrogen bonding toward the thiolate does not influence the strength of the FeO−H bond and the oxidative power of Cpd I. Similar conclusions were drawn

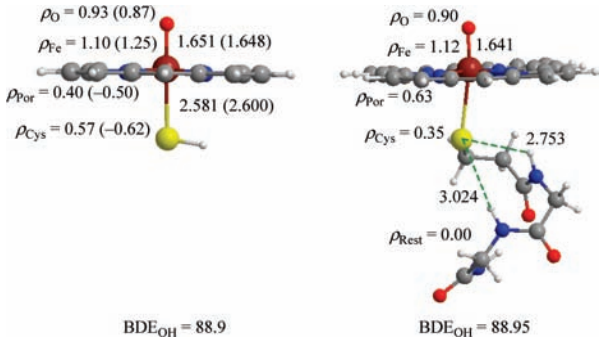

Figure 7. Optimized geometries and group spin densities of Cpd I(SH) and Cpd I with a large axial ligand description using cysteinate and two subsequent amino acids in the chain. Bond lengths are in angstroms and energies in kcal mol^{-1}.

by the Solomon group[32] on a comparison of the BDE_{OH} values between thiolate and imidazole ligated iron(IV)-oxo complexes. Figure 7 displays optimized geometries of two Cpd I models of P450, one with a thiolate ligand and one with an extended axial ligand description. Geometrically, the Fe−O distances are very similar but the Fe−S bond is elongated with a large axial ligand system. The group spin densities on the FeO group (ρ_{Fe} and ρ_O) are the same for both high-spin structures, but in the large model the spin density moves away from the cysteinate group and increases on the porphyrin ring. These spin density changes are in line with previous calculations on enlarged description of the axial group, whereby, e.g., with ammonia molecules pointing toward a thiolate group the electron distribution changed from formally Fe^{IV}═O(Por)($SH^{\bullet}$) to Fe^{IV}═O($Por^{+\bullet}$)(SH^-).[33] Quantum mechanics/molecular mechanics calculations on Cpd I of P450 enzymes give the same effect.[34]

Nonheme enzyme models, such as Cpd I(TauD), have an even higher BDE_{OH} than Cpd I of P450 despite the axially bound histidine group. A DFT calculation on the BDE_{OH} value of a TauD mutant with an axial thiolate group, however, did not increase the BDE_{OH} value significantly and gave an exothermicity of formation of intermediate complexes from a reactant complex of −13.0 kcal mol^{-1}, compared to −15.7 kcal mol^{-1} for the wild-type TauD model. Therefore, the increased BDE_{OH} value of the P450 model with respect to the HRP model is due to the intricate interactions of the thiolate with the porphyrin and not the thiolate ligand on its own. As a consequence nonheme iron(IV)-oxo oxidants do not need a thiolate ligand to enhance their BDE_{OH} value. Interestingly, a much stronger BDE_{OH} is observed for Fe^{IV}(OH)($Por^{+\bullet}$)(OH), which also gives one of the lowest C−H hydroxylation barriers, and therefore should be a particularly strong oxidant.

The calculations described in this work show that replacing the axial ligand in iron(IV)-oxo porphyrin cation radical systems can change the BDE_{OH} value with as much as 20 kcal mol^{-1}. To explain this, we show the orbital energy levels of three oxidants, namely Fe^{IV}═O($Por^{+\bullet}$)L with L = ImH, SH^- and OH^-, in Figure 8, which have BDE_{OH} values of 80.8, 88.9, and 99.5 kcal mol^{-1}, respectively. In order to compare the orbital energy levels of these three oxidants we calculated the energies relative to the $\delta_{x2\text{-}y2}$ orbital, which is the orbital that is located orthogonal to the axial ligand and as a consequence should not be influenced by its perturbations. As follows from the energy levels in Figure 8, the a_{1u} and σ^*_{xy} orbitals are hardly influenced by the nature of the axial ligand, while small changes are seen for the π^*_{xz}, π^*_{yz}, and σ^*_{z2} orbital energy levels. Dramatic changes, however, are found for the orbital energy of the a_{2u} molecular orbital and consequently the HOMO−LUMO energy gap for the β-set of orbitals. Thus, the a_{2u} orbital mixes strongly with a π-orbital on the axial ligand, and the overlap is stronger with an anionic axial ligand.[33a] A larger HOMO−LUMO gap will influence EA_{CpdI} directly, since it reflects the vertical electron affinity of the oxidant. Indeed as recently shown, the regioselectivity of ethylbenzene hydroxylation by Fe^{IV}═O($Por^{+\bullet}$)L with L = Cl^- or $NCCH_3$ is dependent on the axial ligand, whereby oxidants with an anionic ligand preferentially give hydrogen atom abstraction, while those with a neutral ligand fare better for aromatic hydroxylation reactions.[35]

Experimentally, the value of BDE_{OH} is determined from the electron affinity of Cpd I (EA_{CpdI}) and the proton affinity (pK_a) of its one-electron reduced form, eq 4.[36] However, a plot of the barrier height against EA_{CpdI} did not give a linear correlation (Figure S8, Supporting Information), which implies that the electron affinity and pK_a values are coupled in the transition state. Although the HOMO−LUMO energy gaps in Figure 8 give the same trend as BDE_{OH}, the energy differences between the three HOMO−LUMO gaps do not match the BDE_{OH} differences of the three oxidants and as a result the barrier height does not correlate with EA_{CpdI} but with BDE_{OH} only. Consequently, EA_{CpdI} and pK_a combined correlate with barrier height through BDE_{OH}, because the reactions proceed via a hydrogen atom abstraction with simultaneous migration of an electron and a proton in the rate determining step rather than a proton-coupled-electron-transfer, where the proton and electron transfer processes happen sequentially.

By contrast to aliphatic hydroxylation reactions like those studied in this work, in aromatic hydroxylation reactions by iron(IV)-oxo oxidants the reactions proceed via different reaction mechanisms,[35] whereby the rate determining step is a nucleophilic attack of the oxo group on a carbon atom of the aromatic ring. In this process, two electrons are transferred from the substrate to the oxidant in the rate determining step, while the hydrogen atom migration proceeds in a later step in the reaction mechanism. Hence, it may be anticipated that the barrier height of aromatic hydroxylation reactions will not correlate with the strength of the C−H bond of the substrate but more likely with the ionization potential of the substrate and the one- or two-electron reduction potential of the iron(IV)-oxo complex. This shows that aromatic and aliphatic reaction mechanisms follow fundamentally different reaction processes and the regioselectivity of aromatic versus aliphatic hydroxylation may vary when there are different ligands on the metal-oxo oxidant. Indeed, Nam et al. observed a regioselectivity change upon aromatic

(32) Dey, A.; Jiang, Y.; Ortiz de Montellano, P. R.; Hodgson, P. O.; Hedman, B.; Solomon, E. I. *J. Am. Chem. Soc.* **2009**, *131*, 7869–7878.
(33) (a) Ogliaro, F.; Cohen, S.; de Visser, S. P.; Shaik, S. *J. Am. Chem. Soc.* **2000**, *122*, 12892–12893. (b) de Visser, S. P.; Tan, L. S. *J. Am. Chem. Soc.* **2008**, *130*, 12961–12974.
(34) (a) Schöneboom, J. C.; Lin, H.; Reuter, N.; Thiel, W.; Cohen, S.; Ogliaro, F.; Shaik, S. *J. Am. Chem. Soc.* **2002**, *124*, 8142–8151. (b) Bathelt, C. M.; Zurek, J.; Mulholland, A. J.; Harvey, J. N. *J. Am. Chem. Soc.* **2005**, *127*, 12900–12908.
(35) de Visser, S. P.; Tahsini, L.; Nam, W. *Chem.—Eur. J.* **2009**, *15*, 5577–5587.
(36) (a) Friedrich, L. E. *J. Org. Chem.* **1983**, *48*, 3851–3852. (b) Bordwell, F. G.; Cheng, J.-P. *J. Am. Chem. Soc.* **1991**, *113*, 1736–1743. (c) Bordwell, F. G.; Cheng, J.-P.; Ji, G.-Z.; Satish, A. V.; Zhang, X. *J. Am. Chem. Soc.* **1991**, *113*, 9790–9795.

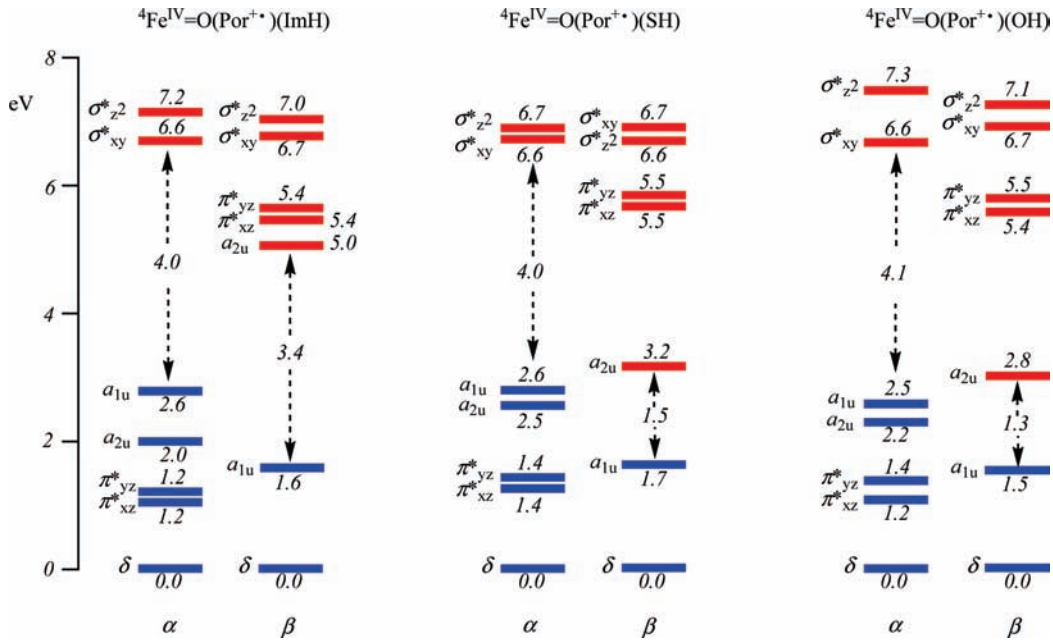

Figure 8. Orbital energies of the orbitals depicted in Figure 2 for Fe^{IV}=O($Por^{+\bullet}$)(ImH), Fe^{IV}=O($Por^{+\bullet}$)(SH) and Fe^{IV}=O($Por^{+\bullet}$)(OH). Energies in eV scaled relative to $\delta_{x2\text{-}y2}$ orbital. Occupied orbitals in blue and virtual orbitals in red.

versus aliphatic hydroxylation of ethylbenzene by an iron(IV)-oxo oxidant with different axial ligands.[37]

$$BDE_{OH} = 23.06EA_{CpdI} + 1.37pK_a + C \quad (4)$$

Recent studies of the Solomon group[32] implicated small but non-negligible effects on the hydrogen abstraction ability of an oxidant, whereby the axial cysteinate ligand of an iron(IV)-oxo porphyrin cation radical model was replaced by imidazole. This resulted in a decrease of about 4 kcal mol^{-1} in BDE_{OH} and hence lower rate constants for imidazole ligated iron-porphyrin complexes in agreement with experimental studies of the Nam group on a series of nonheme iron(IV)-oxo oxidants.[37] Thus, Nam and co-workers used a series of nonheme iron(IV)-oxo complexes with TMC (1,4,8,11-tetramethyl-1,4,8,11-tetraazacyclotetradecane) and variable axial ligand. In a reaction with alkanes the oxidants with neutral axial ligand were the least reactive and those with an anionic ligand system were the most reactive, as also shown in this work. Our models of HRP and P450 are slightly different from those used by the Solomon group, hence the BDE_{OH} differences are somewhat larger, namely 8 kcal mol^{-1}. Moreover, our calculations support experimental studies of the Nam and Fujii groups that showed a pronounced axial ligand effect on substrate hydroxylation and epoxidation by iron(IV)-oxo porphyrin cation radical oxidants, especially when an imidazole ligand was replaced by phenolate.[38]

Correlation of Barrier Height with Intrinsic Properties of Oxidant and Substrate. To test whether the hydrogen abstraction barrier is influenced by intrinsic chemical properties of the oxidant and substrate we calculated the electric polarizability change along the reaction mechanism. A linear correlation was found between atomization enthalpies of analogous molecules with the difference in polarizability volume ($\Delta\alpha_{AV}$) for atomization, eq 5.[39] The polarizability difference is taken as the polarizability of molecule *M* (α_M) minus the sum of the atomic polarizabilities of its contents (α_{atoms}), eq 5.

$$\Delta\alpha_{AV} = \alpha_M - \sum \alpha_{atoms} \quad (5)$$

Here, we took the polarizability trace from the Gaussian frequency calculations and estimated the polarizability difference for the process from reactants to the transition state, by taking the difference in polarizability trace between that for the transition state (α_{TS}) with respect to that for isolated reactants, i.e., Cpd I and substrate (SubH) as follows:

$$\Delta\alpha_{AV} = \alpha_{TS} - \alpha_{CpdI} - \alpha_{SubH} \quad (6)$$

In Figure 9, we depict the barrier heights of substrate hydroxylation with respect to the polarizability difference. Panel (a) gives the data for propene hydroxylation by the range of iron(IV)-oxo complexes shown in Figure 1 and Table 1, while panel (b) displays substrate hydroxylation by Fe^{IV}=O($Por^{+\bullet}$)SH as taken from ref 14. As follows from Figure 9a,b, the polarizability difference correlates linearly with the barrier height for the reaction. In particular, the larger the polarizability change from reactants to transition state, the smaller the barrier height becomes. This implies that the charge distribution in the transition state is important for the total barrier height of the reaction and determines the energy change.

Discussion

So what is the origin of these correlations and how does it compare with the correlation against BDE_{CH} found previously? These questions will be addressed in the next few sections.

The substrate hydroxylation mechanism by iron(IV)-oxo oxidants is described in Figure 10 by a valence bond curve

(37) Sastri, C. V.; Lee, J.; Oh, K.; Lee, Y. J.; Lee, J.; Jackson, T. A.; Ray, K.; Hirao, H.; Shin, W.; Halfen, J. A.; Kim, J.; Que, L., Jr.; Shaik, S.; Nam, W. *Proc. Natl. Acad. Sci. U.S.A.* **2007**, *104*, 19181–19186.

(38) (a) Song, W. J.; Ryu, Y. O.; Song, R.; Nam, W. *J. Biol. Inorg. Chem.* **2005**, *10*, 294–304. (b) Takahashi, A.; Kurahashi, T.; Fujii, H. *Inorg. Chem.* **2009**, *48*, 2614–2625.

(39) de Visser, S. P. *Phys. Chem. Chem. Phys.* **1999**, *1*, 749–753.

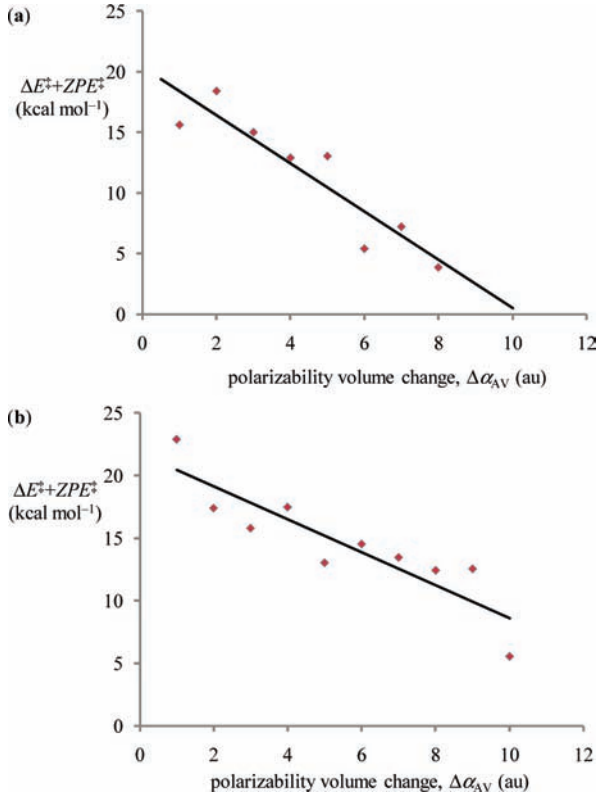

Figure 9. Barrier height of substrate hydroxylation versus polarizability change. (a) Reaction of propene with iron(IV)-oxo oxidants. (b) Substrate hydroxylation by Cpd I(SH). Data for part (b) taken from ref 14.

crossing diagram. In a curve crossing diagram like the one shown in Figure 10, the respective wave functions that represent the electronic configurations of the reactants (Ψ_r) and products (Ψ_p) are considered. Thus, Ψ_r (shown in blue) starts bottom left of the drawing in the reactant geometry and connects to an excited state in the product geometry (Ψ_p*). In a similar way, the product wave function Ψ_p starts in the product geometry and connects to an excited state in the reactant geometry (Ψ_r*).

The Ψ_r and Ψ_p wave functions cross each other and generate an avoided crossing and a concerted barrier for substrate hydroxylation. However, hydrogen abstraction is a stepwise mechanism, where the reactant and product curves are bisected by a third curve, namely the intermediate wave function (Ψ_I) for the radical intermediate. The wave function for the intermediate state in the geometry of the reactants is labeled as Ψ_I*. Thus, the curve crossing diagram shown in Figure 10 gives three curve crossings, namely one between reactants and intermediates (leading to a hydrogen abstraction barrier, $\Delta E_{HA}^{\ddagger}$), one between intermediates and products (to form the rebound barrier, $\Delta E_{reb}^{\ddagger}$) and one that directly links reactants and products (the concerted reaction barrier). The latter is high in energy but due to the existence of an intermediate wave function a low-energy alternative is provided.

The reactant wave function (Ψ_r) and the radical intermediate wave function (Ψ_I) cross each other at an energy ΔE_C above the energy of the reactants that gives rise to an avoided crossing and a hydrogen abstraction transition state. The barrier for this process is $\Delta E_{HA}^{\ddagger}$ which is a factor B below the crossing point ΔE_C. B is the resonance energy in the transition state and is proportional to the HOMO−LUMO energy gap in the transition state.[40] It was shown that the vertical excitation energy in Ψ_r, or promotion gap G_H, is a fraction (f) of ΔE_C, eq 7.[40] The promotion gap G_H for the hydrogen abstraction step in Figure 10, therefore, is dependent on the electron transfer processes from reactants to radical intermediates in the geometry of the reactants. In our previous studies,[14] we showed that G_H is proportional to BDE_{CH} for a series of aliphatic hydroxylation reactions by Fe^{IV}═O($Por^{+\bullet}$)SH, hence a linear correlation between hydrogen abstraction barrier (or rate constant) and BDE_{CH} was found.

$$\Delta E^{\ddagger} = fG_H - B \tag{7}$$

The heme and nonheme iron(IV)-oxo complexes have different electronic configurations and as a consequence different values of G_H are expected. On the left-hand side of Figure 10 we show the two electron distributions of the reactants with

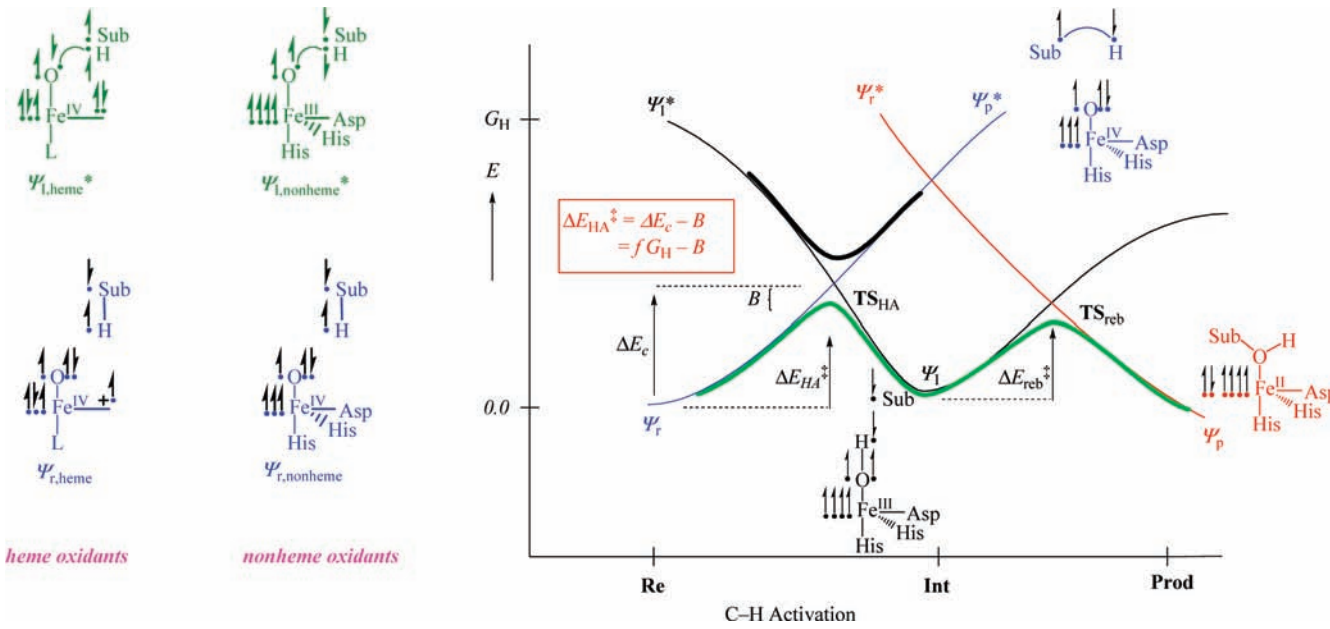

Figure 10. Generalized VB curve crossing diagram for a hydrogen abstraction reaction.

wave function $\Psi_{r,heme}$ and $\Psi_{r,nonheme}$ and the excited state wave functions $\Psi_{I,heme}$* and $\Psi_{I,nonheme}$* for heme and nonheme iron(IV)-oxo oxidants, respectively. Thus, heme oxidants such as Fe^{IV}═O($Por^{+\bullet}$)L have an electronic ground state with occupation $\delta_{x2\text{-}y2}^2\ \pi^*_{xz}{}^1\ \pi^*_{yz}{}^1\ a_{2u}{}^1$. The π^*_{xz} and π^*_{yz} orbitals are antibonding orbitals along the Fe−O bond that generally give rise to a spin density of approximately one on the iron and one on the oxygen atom, hence we depict three electrons next to the iron and one next to the oxygen atom in $\Psi_{r,heme}$ in Figure 10. In addition, there is a lone-pair of electrons identified next to the oxygen atom, a doubly occupied $\delta_{x2\text{-}y2}$ orbital, and an unpaired electron on the heme in the a_{2u} molecular orbital and a pair of electrons in the C−H bond of SubH. For simplicity, the other electrons located on iron and oxygen have been removed from this figure for clarity. Excitation from $\Psi_{r,heme}$ to $\Psi_{I,heme}$* retains the orbital occupation on the metal but leads to an electron transfer from the lone pair on oxygen into the a_{2u} orbital on the porphyrin ring. The other electron of the lone pair on oxygen forms a bond with the electron of the hydrogen atom into an O−H bond, while at the same time the C−H bond breaks to form a Sub radical. Thus, from the interactions of the electrons in $\Psi_{r,heme}$ and $\Psi_{I,heme}$* it follows that the excitation energy is proportional to the singlet−triplet coupling in the C−H bond of the substrate ($E_{ST,CH}$), the singlet−triplet coupling in the O−H bond of the iron-hydroxo complex ($E_{ST,OH}$) and the excitation energy of an electron from the lone pair on oxygen into the a_{2u} orbital ($E_{lp\rightarrow a2u}$), eq 8.

$$G_{H,heme} = E_{ST,CH} - E_{ST,OH} + E_{lp\rightarrow a2u} \quad (8)$$

The singlet−triplet energy of electrons in a C−H bond is proportional to BDE_{CH},[41] and the singlet−triplet energy of electrons in the O−H bond to BDE_{OH}. Consequently, G_H is proportional to the difference in energy between BDE_{CH} and BDE_{OH}, and as a result also the barrier height of the hydrogen abstraction reaction, eq 9.

$$\Delta E_{HA,heme}{}^{\ddagger} = f(BDE_{CH} - BDE_{OH} + E_{lp\rightarrow a2u}) + B \quad (9)$$

In nonheme iron(IV)-oxo oxidants the electronic quintet spin state has configuration $\delta_{x2\text{-}y2}{}^1\ \pi^*_{xz}{}^1\ \pi^*_{yz}{}^1\ \sigma^*_{xy}{}^1$. Also here the two π^* orbitals give a spin density of 50% on iron and 50% on oxygen, so that we allocate three unpaired electrons with up-spin to the metal and one with up-spin to oxygen in $\Psi_{r,nonheme}$. No unpaired spins are located on the metal ligands in nonheme iron(IV)-oxo species. Similar to the discussion above for heme iron(IV)-oxo oxidants, it follows from the electron distributions shown in Figure 10 that the promotion gap for nonheme iron(IV)-oxo oxidants is dependent on the singlet−triplet energy of the electrons in the O−H ($E_{ST,OH}$) and C−H ($E_{ST,CH}$) bonds. In addition, the promotion gap contains a contribution for the excitation energy of an electron from the lone-pair on oxygen into the σ^*_{xy} molecular orbital, eq 10. The correlations shown above in Figure 6 appear to be very little affected by the excitation energy ($E_{lp\rightarrow a2u}$ or $E_{lp\rightarrow \sigma^*xy}$), which implies that this factor is small. Indeed, the resonance energy (B in eq 9 and B' in eq 10) contain a contribution for the HOMO−LUMO excitation energy in the transition state,[42] which is proportional to this excitation energy from the lone pair on oxygen, and hence this contribution cancels out.

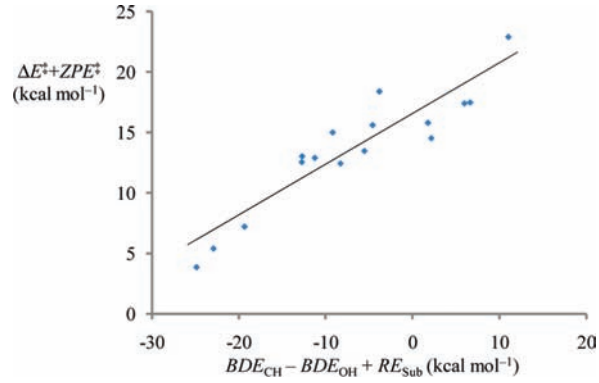

Figure 11. Correlation of the hydrogen abstraction barrier height and reaction enthalpy for a series of hydrogen abstraction reactions. Data taken from ref 14 for P450 hydroxylation reactions and this work for propene hydroxylation by iron(IV)-oxo oxidants.

$$\Delta E_{HA,heme}{}^{\ddagger} = f'(BDE_{CH} - BDE_{OH} + E_{lp\rightarrow\sigma^*xy}) + B' \quad (10)$$

This VB model, therefore, explains the origin of the correlations of hydrogen abstraction rate constant with either BDE_{CH} or BDE_{OH} as observed experimentally and is in agreement with the correlation displayed in Figure 6. As a matter of fact the correlation of hydrogen abstraction barrier with the difference between BDE_{CH} and BDE_{OH} also implies a linear correlation between the barrier height of hydrogen abstraction with the reaction energy of hydrogen abstraction, i.e. $\Delta E^{\ddagger} \propto \Delta H_r$, eq 11. This type of correlation has been anticipated by the Polanyi theory and is proven here for hydrogen atom abstraction reactions by metal-oxo oxidants.[43] Indeed, a plot of all hydrogen abstraction reactions discussed in this work combined with the substrate hydroxylation reactions by Fe^{IV}═O($Por^{+\bullet}$)SH as reported in ref 14 gives a linear correlation between the calculated barrier height and the reaction enthalpy (Figure 11) as suggested by the VB model shown above. The value of ΔH_r is calculated from the difference in BDE_{CH} and BDE_{OH} (eq 2 above) and corrected for RE_{Sub}. Clearly, the substrates that give the strongest exothermicity for hydrogen atom abstraction give the lowest hydrogen atom abstraction barriers in agreement with the Polanyi equation and the VB mechanism shown above.

$$\Delta E^{\ddagger} \propto BDE_{CH} - BDE_{OH} = \Delta H_r \quad (11)$$

To test the VB diagram and find out whether it has predictive value we estimated the propene hydroxylation barriers from empirical data, see Table 2. We used two methods based on eq 7 to estimate the barriers and these obtained results are given as $\Delta E^{\ddagger}_{VB1}$ and $\Delta E^{\ddagger}_{VB2}$ in Table 2. In the first method we calculate G_H from twice the value of the bond energy of the O−H bond (corrected with RE_{Sub} and RE_{FeOH}). In addition, B is taken as the weaker of the two bonds (either the C−H or O−H) that is broken or formed. In our case, all values (except

(40) (a) Shaik, S. S. *J. Am. Chem. Soc.* **1981**, *103*, 3692–3701. (b) Shaik, S.; Shurki, A. *Angew. Chem., Int. Ed.* **1999**, *38*, 586–625.
(41) Shaik, S.; Hiberty, P. C. *A Chemist's Guide to Valence Bond Theory*; Wiley-Interscience: New York, NY, 2007.
(42) (a) Song, L.; Wu, W.; Dong, K.; Hiberty, P. C.; Shaik, S. *J. Phys. Chem. A* **2002**, *106*, 11361–11370. (b) Su, P.; Song, L.; Wu, W.; Hiberty, P. C.; Shaik, S. *J. Am. Chem. Soc.* **2004**, *126*, 13539–13549.
(43) (a) Evans, M. G.; Polanyi, M. *Trans. Faraday Soc.* **1936**, *32*, 1333–1360. (b) Evans, M. G.; Polanyi, M. *Trans. Faraday Soc.* **1938**, *34*, 11–29. (c) Butler, E. T.; Polanyi, M. *Trans. Faraday Soc.* **1943**, *39*, 19–36.

Table 2. Estimated Hydrogen Abstraction Barriers for the Reverse Reaction FeOH + Sub$^{\bullet}$ → Fe^{IV}=O + SubH from Empirical Calculations

oxidant	$\Delta E^{\ddagger}_{HA,rev}$[a]	$\Delta E^{\ddagger}_{VB1}$[b]	$\Delta E^{\ddagger}_{VB2}$[c]
Fe^{IV}=O($Por^{+\bullet}$)ImH	19.6	16.8	15.2
Cpd I(C*c*P)	18.4	15.4	14.7
Fe^{IV}=O(TMCS)$^{+}$	17.4	15.6	15.0
Fe^{IV}=O($Por^{+\bullet}$)Cl	17.7	17.7	17.3
Fe^{IV}=O($Por^{+\bullet}$)SH	19.1	17.2	16.8
Cpd I(TauD)	21.1	25.1	25.6
Fe^{IV}=O(N4Py)$^{2+}$	23.6	23.3	23.6
Fe^{IV}=O($Por^{+\bullet}$)OH	20.2	27.9	28.8

[a] Calculated from the difference in energy of $\mathbf{TS}_{HA}$ and RadInt. [b] Using $f_{av} = 0.27 \pm 0.02$. [c] Using $B_{av} = 48.9 \pm 4.4$ kcal mol^{-1}.

that for the HRP CpdI model) have $B = BDE_{CH}/2$. These values of G_H and B are used together with the reverse hydrogen abstraction barrier ($\Delta E^{\ddagger}_{HA,rev}$) to calculate f, which gives the average value f_{av} for the series of hydrogen atom abstraction reactions. The values of f_{av}, G_H and B are subsequently used to calculate $\Delta E^{\ddagger}_{VB1}$ from eq 7. Note that the reverse hydrogen abstraction barrier ($\Delta E^{\ddagger}_{HA,rev}$) for $\mathbf{TS}_{HA}$ is the energy difference between the hydrogen abstraction barrier ($\mathbf{TS}_{HA}$) and the radical intermediate. In a second set of calculations we use $f = 0.3$ together with $\Delta E^{\ddagger}_{HA,rev}$ and G_H to calculate B. From these values of B, the average is taken (B_{av}), which is inserted into eq 7 together with $f = 0.3$ and G_H to get $\Delta E^{\ddagger}_{VB2}$.

As follows from a comparison of the VB estimated barriers and the DFT calculated barriers, there is reasonable agreement. The average deviation of the barrier heights from the DFT calculations is only 0.2 and 0.0 kcal mol^{-1} for model 1 and 2, respectively, with a standard deviation of 3.7 and 4.4 kcal mol^{-1}. These values drop below 3 kcal mol^{-1} if the datum for Fe^{IV}=O($Por^{+\bullet}$)OH is ignored from the statistics. Consequently, the VB models generally predict hydrogen abstraction trends of iron(IV)-oxo oxidants from empirical values within the error of our computational methods.

In summary, we show that the rate constant of hydrogen abstraction by iron(IV)-oxo complexes correlates linearly with the strength of the C−H bond broken as well as the O−H bond formed. As a consequence, the barrier height of hydrogen abstraction is linearly related to the reaction energy of hydrogen abstraction. These trends have been generalized by a VB curve crossing diagram that explains the barrier height through electron transfer processes.

Conclusions

DFT calculations on propene hydroxylation by a range of iron(IV)-oxo complexes predicts a linear correlation of hydrogen atom abstraction barrier height with the strength of the C−H bond of the substrate (BDE_{CH}) and the strength of the O−H bond of the FeOH complex formed (BDE_{OH}). As a consequence, the barrier height is proportional to the exothermicity of hydrogen atom abstraction in agreement with the Polanyi equations. We have set up a VB curve crossing diagram that explains the trends using electron transfer processes that confirms the observed correlations. Moreover, the VB model gives predictive values of hydrogen abstraction barriers in reasonable agreement with DFT.

Acknowledgment. The National Service of Computational Chemistry Software (NSCCS) is thanked for providing CPU time.

Supporting Information Available: Details of computational methods as well as optimized geometries, absolute and relative energies, group charges and spin densities of all structures described in this work and ref 16 in full. This material is available free of charge via the Internet at http://pubs.acs.org.

JA908340J